Int. J. Appl. Math. Comput. Sci., 2014, Vol. 24, No. 2, 405–415
DOI: 10.2478/amcs-2014-0031

amcs

AN EFFICIENT ALGORITHM FOR ADAPTIVE TOTAL VARIATION BASED IMAGE DECOMPOSITION AND RESTORATION

XINWU LIU [*], LIHONG HUANG [**,***]

[*] School of Mathematics and Computational Science
Hunan University of Science and Technology, Xiangtan, Hunan 411201, China
e-mail: lxinwu@163.com

[**]College of Mathematics and Econometrics
Hunan University, Changsha, Hunan 410082, China

[***]Department of Information Technology
Hunan Women's University, Changsha, Hunan 410004, China

With the aim to better preserve sharp edges and important structure features in the recovered image, this article researches an improved adaptive total variation regularization and H^{-1} norm fidelity based strategy for image decomposition and restoration. Computationally, for minimizing the proposed energy functional, we investigate an efficient numerical algorithm—the split Bregman method, and briefly prove its convergence. In addition, comparisons are also made with the classical OSV (Osher–Sole–Vese) model (Osher *et al.*, 2003) and the TV-Gabor model (Aujol *et al.,* 2006), in terms of the edge-preserving capability and the recovered results. Numerical experiments markedly demonstrate that our novel scheme yields significantly better outcomes in image decomposition and denoising than the existing models.

Keywords: image decomposition, image restoration, adaptive total variation, H^{-1} norm, split Bregman method.

1. Introduction

The subject of image restoration plays an extremely important role in image processing and computer vision. Given a contaminated image f, image reconstruction aims at extracting the true image u from f. Solving this inverse problem, one classical mathematical technique known as the Total Variation (TV) regularization based minimization scheme (the Rudin–Osher–Fatemi (ROF) model), originally introduced by Rudin *et al.* (1992), can be described as

$$\inf_u \int_\Omega |\nabla u| + \frac{\lambda}{2}\int_\Omega |f-u|^2\,\mathrm{d}x, \tag{1}$$

where λ is a tuning parameter. Numerical experiments demonstrate the capability of the model (1) for sufficiently suppressing additive Gaussian noise, while preserving the edge features. Furthermore, to better maintain the fine details and junctions, the adaptive TV approach (Chen and Wunderli, 2002; Barcelos and Chen, 2000; Strong and Chan, 1996) and the edge adaptive weighted regularization scheme (Prasath, 2011) were proposed for image restoration. Thereinto, the adaptive TV strategy can be formulated by

$$\inf_u \int_\Omega \alpha(x)|\nabla u| + \frac{\lambda}{2}\int_\Omega |f-u|^2\,\mathrm{d}x, \tag{2}$$

where $\alpha(x)$ represents a diffusivity function, used for controlling the intensity of the diffusion. Generally, $\alpha(x)$ can be chosen as

$$\alpha(x) = \frac{1}{1+\mathcal{K}|\nabla G_\sigma * f|^2},$$

where $\mathcal{K}$ acts as an edge strength threshold factor, and

$$G_\sigma(x) = \frac{1}{2\pi\sigma^2}\exp\Big(-\frac{|x|^2}{2\sigma^2}\Big)$$

stands for the Gaussian kernel with parameter σ.

Unfortunately, for texture image decomposition, the models mentioned above cannot completely separate the structural component u from the textural component v. Therefore, Meyer (2002) introduced the G norm based

image decomposition model

$$\inf_u \Big\{ \int_\Omega |\nabla u| + \frac{\lambda}{2}\|v\|_*, f = u + v \Big\}, \tag{3}$$

with

$$\|v\|_* = \inf_{g=(g_1,g_2)} \Big\{ \|\sqrt{g_1^2 + g_2^2}\|_{L^\infty} | v = \partial_x g_1 + \partial_y g_2 \Big\}$$

in the G space, where the G space is characterized by

$$G = \{v | v = \partial_x g_1(x,y) + \partial_y g_2(x,y), g_1, g_2 \in L^\infty(\Omega)\}.$$

To easily compute the numerical solution of (3), Vese and Osher (2003) adopted the L^p norm to approximate the $*$ norm, and formulated a novel model

$$\begin{aligned} \inf_{u,g_1,g_2} \Big\{ \int_\Omega |\nabla u| + \frac{\lambda}{2}\int_\Omega |f - u - \mathrm{div}(\vec{g})|^2 \mathrm{d}x \\ + \mu \Big[\int_\Omega (\sqrt{g_1^2 + g_2^2})^p \mathrm{d}x \Big]^{\frac{1}{p}} \Big\}, \end{aligned} \tag{4}$$

where λ, μ are trade-offs to balance three terms, and $p \geq 1$. In (4), by choosing $\vec{g} = \nabla g$, $f - u = v = \mathrm{div}(\vec{g})$ and using the norm in $H^{-1}(\Omega)$, Osher *et al.* (2003) investigated a simplified and modified version ($p = 2$, the OSV model) as

$$\inf_u \int_\Omega |\nabla u| + \frac{\lambda}{2}\int_\Omega |\nabla \Delta^{-1}(f - u)|^2 \mathrm{d}x, \tag{5}$$

and employed the steepest descent method to solve it effectively. Subsequently, Daubechies and Teschke (2005) investigated a variational model for image decomposition and restoration by means of wavelets. Aujol *et al.* (2006) firstly took advantage of the Gabor wavelets functions, and proposed a new TV-Gabor model for structure-texture image decomposition. Compared with the results by the ROF method, the H^{-1} norm based OSV model (5) and the TV-Gabor model can maintain more structure features, and yield better recovered images.

Meanwhile, Chan *et al.* (2007) combined higher order derivatives, and developed the CEP-H^{-1} model for image decomposition. Computationally, they applied dual methods (Aujol *et al.*, 2005; Chambolle, 2004; Chan *et al.*, 1999) to obtain the optimum solution quickly, and demonstrated that this model can be used for substantially reducing the staircasing in the structure component. Lately, a coupled variational model for decomposing and restoring a structure-texture image with blurry and missing pixels has been developed and studied in detail by Ng *et al.* (2013).

In this paper, inspired by the above models (2) and (5), we investigate the spatially and scale adaptive TV minimization model for edge-preserving image decomposition and restoration as follows

$$\inf_u \int_\Omega \alpha(x)|\nabla u| + \frac{\lambda}{2}\int_\Omega |\nabla \Delta^{-1}(f - u)|^2 \mathrm{d}x, \tag{6}$$

where $\alpha(x)$ denotes a spatially and scale adaptive parameter defined the same as in (2), for regulating the degree of smoothing.

Our contributions can be summarized as the following two points. Firstly, the proposed edge-preserving regularization scheme performs better in maintaining essential edges and structures than the two TV regularization based models. Secondly, to evidently speed up the energy minimization for (6), this paper propounds the fast split Bregman algorithm to derive its optimum solution. Mathematically speaking, the steepest descent algorithm is generally very slow, owing to the nonlinearity and strict restrictions on the Courant–Friedrichs–Lewy (CFL) condition. However, our proposed split algorithm computes the non-differentiable item and the squared H^{-1} norm item, respectively. Thus it dramatically accelerates the computational speed.

The remainder of this paper is arranged in the following manner. In Section 2, we describe the necessary preparations about the model (6). The numerical method for solving our novel strategy is investigated and proved in Sections 3 and 4, respectively. Numerical experiments intended for demonstrating the efficiency of the proposed method are provided in Section 5. Finally, concluding remarks are summarized in Section 6.

2. Preliminaries

In this section, our objective is to describe the necessary preparations on the model (6). According to Chen and Wunderli (2002), we now tersely represent two basic theories below.

Definition 1. Let $\Omega \subseteq \mathbb{R}^N$ be a bounded open domain. Let $u \in L^1_{\mathrm{loc}}(\Omega)$, and $\alpha(x) \geq 0$ be a continuous and real function. Then the α-*total variation* of u is defined as

$$\begin{aligned} \int_\Omega \alpha|\nabla u| = \sup_{\phi \in C_c^1(\Omega,\mathbb{R}^N)} \Big\{ \int_\Omega u(x)\mathrm{div}\phi(x)\,\mathrm{d}x : \\ |\phi_i(x)| \leq \alpha(x), \forall x \in \Omega, 1 \leq i \leq n \Big\}, \end{aligned} \tag{7}$$

where ϕ is a vector-valued function $\phi = (\phi_1, \ldots, \phi_n)$. Furthermore, the α-BV seminorm is characterized by

$$\|u\|_{\alpha - BV(\Omega)} = \int_\Omega \alpha|\nabla u| + \|u\|_{L^1(\Omega)}.$$

Theorem 1. (Lower semicontinuity) *Assume that*

$$\{u_i\}_{i=1}^\infty \subset L^1(\Omega)$$

and

$$u_i \to u \quad in\ L^1(\Omega).$$

Then we have

$$\int_\Omega \alpha|\nabla u| \leq \liminf_{i\to\infty} \int_\Omega \alpha|\nabla u_i|. \tag{8}$$

Combining lower semicontinuity for the α-BV seminorm and Theorem 2.3 of Osher *et al*. (2003), we establish the existence of the minimizers for the variational model (6) as follows.

Theorem 2. *Suppose that* $f \in BV(\Omega) + \{v \in L^2(\Omega), \int_\Omega v(x)\,\mathrm{d}x = 0\}$. *Then the minimization problem*

$$\inf_u \Big\{ \int_\Omega \alpha|\nabla u| + \frac{\lambda}{2}\int_\Omega |\nabla\Delta^{-1}(f-u)|^2 \mathrm{d}x, \int_\Omega (f-u)\mathrm{d}x = 0\Big\}, \tag{9}$$

has a solution $u \in BV(\Omega)$.

3. Computational method

For quickly solving the optimization problem (6), in this section we elaborate on a fast numerical algorithm: the split Bregman iteration.

The split Bregman method was initially introduced and studied in image processing by Goldstein and Osher (2009), and the corresponding convergence analysis was exhibited by Cai *et al*. (2009) and Jia *et al*. (2009). Due to its high efficiency and robustness, various applications of this fast iteration algorithm have been reported in image restoration (Cai *et al.*, 2009; Jia *et al.*, 2009; Liu and Huang, 2010; 2012; 2013; 2014; Setzer *et al.*, 2010), hyperspectral images analysis (Szlam *et al*., 2010), and compressed sensing (Zhang *et al*., 2009), etc.

Here the split Bregman method is campaigned to solve the following optimization problem:

$$\hat{u} = \arg\min_u \Big\{ \|\alpha\nabla u\|_1 + \frac{\lambda}{2}\|\nabla\Delta^{-1}(f-u)\|_2^2 \Big\}. \tag{10}$$

Firstly, we take the effective replacement $\nabla u \to d$. By introducing the auxiliary variable d, this leads to a constrained optimization problem

$$\min_{u,d} \|d\|_1 + \frac{\lambda}{2}\|\nabla\Delta^{-1}(f-u)\|_2^2, \ \ s.t.\ d = \alpha\nabla u, \tag{11}$$

which can be reduced to the following equivalent unconstrained formulations:

$$(u^{k+1}, d^{k+1}) = \arg\min_{u,d} \|d\|_1 + \frac{\lambda}{2}\|\nabla\Delta^{-1}(f-u)\|_2^2 + \frac{\gamma}{2}\|d - \alpha\nabla u - b^k\|_2^2, \tag{12}$$

with the update formula for b^{k+1}

$$b^{k+1} = b^k + (\alpha\nabla u^{k+1} - d^{k+1}). \tag{13}$$

Since u, d are decoupled together as shown in (12), it can be transformed into two subproblems as follows:

$$u^{k+1} = \arg\min_u \frac{\lambda}{2}\|\nabla\Delta^{-1}(f-u)\|_2^2 + \frac{\gamma}{2}\|\alpha\nabla u - d^k + b^k\|_2^2, \tag{14}$$

$$d^{k+1} = \arg\min_d \|d\|_1 + \frac{\gamma}{2}\|d - \alpha\nabla u^{k+1} - b^k\|_2^2, \tag{15}$$

$$b^{k+1} = b^k + (\alpha\nabla u^{k+1} - d^{k+1}). \tag{16}$$

Numerically computing (14), we derive the following optimality condition for u^{k+1}:

$$0 = \lambda\Delta^{-1}(u^{k+1} - f) + \gamma\nabla^T(\alpha\nabla u^{k+1} - d^k + b^k), \tag{17}$$

which implies that

$$\Big(\frac{\lambda}{\gamma}\Delta^{-1} - \alpha\Delta\Big)u^{k+1} = \frac{\lambda}{\gamma}\Delta^{-1}f + \mathrm{div}(b^k - d^k), \tag{18}$$

where $\nabla^T = -\mathrm{div}$ and $\Delta = -\nabla^T\nabla$. Noticing that the system (18) is linear and symmetric positive definite, the subproblem for u^{k+1} can be efficiently solved by the fast Fourier transform. Denoting by $\mathcal{F}(u)$ the Fourier transform of u, we obtain the solution of the u subproblem as

$$u^{k+1} = \mathcal{F}^{-1}\left(\frac{\frac{\lambda}{\gamma}\mathcal{F}(\Delta^{-1})\circ\mathcal{F}(f) + \mathcal{F}(\hat{D}_x^-)\circ\mathcal{F}(b_x^k - d_x^k)}{\frac{\lambda}{\gamma}\mathcal{F}(\Delta^{-1}) - \mathcal{F}(\alpha)\circ\mathcal{F}(\Delta)} + \frac{\mathcal{F}(\hat{D}_y^-)\circ\mathcal{F}(b_y^k - d_y^k)}{\frac{\lambda}{\gamma}\mathcal{F}(\Delta^{-1}) - \mathcal{F}(\alpha)\circ\mathcal{F}(\Delta)} \right), \tag{19}$$

where "$\circ$" stands for the componentwise multiplication, $\hat{D}_x^-, \hat{D}_y^-$ and $\Delta = \hat{D}_x^-\hat{D}_x^+ + \hat{D}_y^-\hat{D}_y^+$ respectively denote the Fourier transform operators of their corresponding convolution kernels.

Motivated by the techniques of Goldstein and Osher (2009) as well as Wang *et al*. (2007), here we employ the generalized shrinkage formula to deal with the subproblem (15), which is outlined as follows:

$$\begin{aligned} d^{k+1} &= \mathrm{shrink}(\alpha\nabla u^{k+1} + b^k, \frac{1}{\gamma}) \\ &= \max(\|\alpha\nabla u^{k+1} + b^k\|_1 - \frac{1}{\gamma}, 0) \\ &\quad \times \frac{\alpha\nabla u^{k+1} + b^k}{\|\alpha\nabla u^{k+1} + b^k\|_1}. \end{aligned} \tag{20}$$

In summary, the optimization problem (10) can be effectively solved via the alternating minimization method, which is formulated as Algorithm 1.

Algorithm 1. Split Bregman iteration for solving the ATV-H^{-1} model.

Initialization: $u^0 = \mathcal{F}^{-1}(f)$, and $d^0 = b^0 = 0$;
while $\|u^{k+1} - u^k\|_2/\|u^{k+1}\|_2 > tol$
  for $n = 1$ to N
    u^{k+1}
    $$= \mathcal{F}^{-1}\Big(\frac{\frac{\lambda}{\gamma}\mathcal{F}(\Delta^{-1}) \circ \mathcal{F}(f) + \mathcal{F}(\hat{D}_x^-) \circ \mathcal{F}(b_x^k - d_x^k)}{\frac{\lambda}{\gamma}\mathcal{F}(\Delta^{-1}) - \mathcal{F}(\alpha) \circ \mathcal{F}(\Delta)} + \frac{\mathcal{F}(\hat{D}_y^-) \circ \mathcal{F}(b_y^k - d_y^k)}{\frac{\lambda}{\gamma}\mathcal{F}(\Delta^{-1}) - \mathcal{F}(\alpha) \circ \mathcal{F}(\Delta)}\Big)$$
    $d^{k+1} = \max(\|\alpha\nabla u^{k+1} + b^k\|_1 - \frac{1}{\gamma}, 0)\frac{\alpha\nabla u^{k+1} + b^k}{\|\alpha\nabla u^{k+1} + b^k\|_1}$
  end
  $b^{k+1} = b^k + (\alpha\nabla u^{k+1} - d^{k+1})$
end

Similarly as in the work of Goldstein and Osher (2009), the above alternating minimization algorithm with larger N not only is unable to accelerate the convergence evidently, but also deteriorates the accuracy of the inner loop. As a result, we simply fix $N = 1$ in the above algorithm throughout the experiments. As we shall see below, an appropriate stopping criterion may inductively generate a satisfactory recovered result by a few numbers of outer iterations.

4. Convergence analysis

This section is devoted to proving the convergence of the proposed split Bregman method.

Theorem 3. *Let $\{u^k, d^k, b^k\}_{k\in\mathbb{N}}$ be the sequence generated by the iterative process (14)–(16). Then the accumulation point of u^k is a solution to (6).*

Proof. Let us assume that u^* is a solution to (6), and the sequence $\{u^k, d^k, b^k\}_{k\in\mathbb{N}}$ is generated by the proposed algorithm. Thanks to Cai *et al*. (2009) as well as Liu and Huang (2010), the first order optimality conditions for (14)–(16) can be characterized by

$$\begin{cases} q^{k+1} + \gamma\nabla^T(\alpha\nabla u^{k+1} - d^k + b^k) = 0, \\ p^{k+1} + \gamma(d^{k+1} - \alpha\nabla u^{k+1} - b^k) = 0, \\ b^{k+1} = b^k + (\alpha\nabla u^{k+1} - d^{k+1}), \end{cases} \tag{21}$$

where $p^k \in \partial\|d^k\|_1$, and $q^k \in \partial H(u^k)$ with $H(u) = \frac{\lambda}{2}\|\nabla\Delta^{-1}(f - u)\|_2^2$.

Meanwhile, the Karush–Kuhn–Tucker (KKT) conditions for (6) lead to the following result:

$$-\operatorname{div} p^* + q^* = 0, \tag{22}$$

where $q^* \in \partial H(u^*)$, and $p^* \in \partial\|d^*\|_1$ with $d^* = \alpha\nabla u^*$.

Letting $b^* = \frac{1}{\gamma}p^*$ and substituting it into (21), we obtain

$$\begin{cases} q^* + \gamma\nabla^T(\alpha\nabla u^* - d^* + b^*) = 0, \\ p^* + \gamma(d^* - \alpha\nabla u^* - b^*) = 0, \\ b^* = b^* + (\alpha\nabla u^* - d^*), \end{cases} \tag{23}$$

which asserts that $\{u^*, d^*, b^*\}$ is a fixed point of (21).

In what follows, we denote the errors by $u_e^k = u^k - u^*$, $d_e^k = d^k - d^*$, and $b_e^k = b^k - b^*$. All equations of (21) subtracted from those of (23) correspondingly show that

$$\begin{cases} q_e^{k+1} + \gamma\nabla^T(\alpha\nabla u_e^{k+1} - d_e^k + b_e^k) = 0, \\ p_e^{k+1} + \gamma(d_e^{k+1} - \alpha\nabla u_e^{k+1} - b_e^k) = 0, \\ b_e^{k+1} = b_e^k + (\alpha\nabla u_e^{k+1} - d_e^{k+1}). \end{cases} \tag{24}$$

Pre- and post-multiplying the first two equations of (24) by αu_e^{k+1} and d_e^{k+1} and squaring both the sides of the last one, we have

$$\begin{cases} \langle q^{k+1} - q^*, \alpha u_e^{k+1}\rangle + \gamma\langle\nabla^T(\alpha\nabla u_e^{k+1}), \alpha u_e^{k+1}\rangle \\ \qquad +\gamma\langle\alpha u_e^{k+1}, \nabla^T b_e^k - \nabla^T d_e^k\rangle = 0, \\ \langle p^{k+1} - p^*, d_e^{k+1}\rangle + \gamma\|d_e^{k+1}\|_2^2 \\ \qquad -\gamma\langle d_e^{k+1}, \alpha\nabla u_e^{k+1} + b_e^k\rangle = 0, \\ \|b_e^{k+1}\|_2^2 = \|b_e^k\|_2^2 + \|\alpha\nabla u_e^{k+1} - d_e^{k+1}\|_2^2 \\ \qquad +2\langle b_e^k, \alpha\nabla u_e^{k+1} - d_e^{k+1}\rangle. \end{cases} \tag{25}$$

From (25), we have that

$$\begin{aligned} &\frac{\gamma}{2}[(\|b_e^k\|_2^2 - \|b_e^{k+1}\|_2^2) + (\|d_e^k\|_2^2 - \|d_e^{k+1}\|_2^2)] \\ &= \langle q^{k+1} - q^*, \alpha u_e^{k+1}\rangle + \langle p^{k+1} - p^*, d_e^{k+1}\rangle \\ &\quad + \frac{\gamma}{2}\|\alpha\nabla u_e^{k+1} - d_e^k\|_2^2. \end{aligned} \tag{26}$$

Summing (26) from $k = 0$ to $k = K$, we get

$$\begin{aligned} &\frac{\gamma}{2}[(\|b_e^0\|_2^2 - \|b_e^{K+1}\|_2^2) + (\|d_e^0\|_2^2 - \|d_e^{K+1}\|_2^2)] \\ &= \sum_{k=0}^{K}\langle q^{k+1} - q^*, \alpha u_e^{k+1}\rangle + \sum_{k=0}^{K}\langle p^{k+1} - p^*, d_e^{k+1}\rangle \\ &\quad + \frac{\gamma}{2}\sum_{k=0}^{K}\|\alpha\nabla u_e^{k+1} - d_e^k\|_2^2. \end{aligned} \tag{27}$$

This means that the three items located on the right-hand side of (27) are bounded. Subsequently, this

yields the following fact

$$\begin{cases} \lim\limits_{k\to\infty} \langle q^k - q^*, \alpha(u^k - u^*)\rangle = 0, \\ \lim\limits_{k\to\infty} \langle p^k - p^*, d^k - d^*\rangle = 0, \end{cases} \tag{28}$$

The definition of the Bregman distance, together with $d^* = \alpha\nabla u^*$, gives

$$\lim_{k\to\infty} \|\alpha\nabla u^k - d^k\|_2^2 = 0.$$

Furthermore, we have

$$\lim_{k\to\infty} \|\alpha\nabla u^k\|_1 - \|\alpha\nabla u^*\|_1 - \langle p^*, \alpha(\nabla u^k - \nabla u^*)\rangle = 0. \tag{29}$$

Similarly, we obtain

$$\lim_{k\to\infty} H(u^k) - H(u^*) - \langle \alpha(u^k - u^*), q^*\rangle = 0. \tag{30}$$

By (29) and (30), it follows that

$$\lim_{k\to\infty} (\|\alpha\nabla u^k\|_1 + H(u^k)) - (\|\alpha\nabla u^*\|_1 + H(u^*)) - \langle \alpha(u^k - u^*), \nabla^T p^* + q^*\rangle = 0. \tag{31}$$

This, together with (22), implies

$$\lim_{k\to\infty} \|\alpha\nabla u^k\|_1 + H(u^k) = \|\alpha\nabla u^*\|_1 + H(u^*), \tag{32}$$

which indicates that $u^k \to u^*$ as $k \to \infty$. This concludes the proof. ■

5. Numerical results

To illustrate the performance and superiority of our new method for edge-preserving image decomposition and restoration, four interrelated numerical experiments are presented, and comparisons are also made with the state-of-the-art OSV model and TV-Gabor model in detail. Computationally, we efficiently solve the TV-Gabor model by employing the classical projection algorithm (Chambolle, 2004; Aujol and Gilboa, 2006), while the OSV model and our addressed model via the split Bregman algorithm, respectively. Moreover, all experiments were implemented using MATLAB 7.8 (R2009a) for Windows 7, on a PC with an Intel(R) Core(TM) i5 CPU and 4 GB of RAM.

Furthermore, the criterion for stopping the split Bregman iteration relies on the difference between the consecutive iterations of the restored results, which can be summarized in the following formulation:

$$\frac{\|u^{k+1} - u^k\|_2}{\|u^{k+1}\|_2} < 10^{-3}. \tag{33}$$

We evaluate the performance of different approaches, by computing the Signal to Noise Ratio (SNR) and the Peak Signal to Noise Ratio (PSNR) in the recovered images characterized by

$$\mathrm{SNR} = 10 \cdot \log_{10}\left(\frac{\sum_\Omega (u_{i,j} - \bar{u}_{i,j})^2}{\sum_\Omega (n_{i,j} - \bar{n}_{i,j})^2}\right), \tag{34}$$

$$\mathrm{PSNR} = 10 \cdot \log_{10}\left(\frac{255^2 \times M \times N}{\sum\limits_{i=1}^{M}\sum\limits_{j=1}^{N} (u_{i,j} - \tilde{u}_{i,j})^2}\right), \tag{35}$$

where $u_{i,j}$ and $\tilde{u}_{i,j}$ denote the original image and the restored one, $\bar{u}_{i,j}$ and $\bar{n}_{i,j}$ indicate the expectations of the image and the additive noise, respectively, and $M \times N$ stands for the image size. Generally, the larger the SNR (dB) and PSNR (dB) values, the better the performance.

Following Hajiaboli (2010) and Liu *et al*. (2011), we also evaluate the edge-preserving ability of different schemes by measuring Pratt's Figure Of Merit (FOM) in the recovered image, defined as

$$\mathrm{FOM} = \frac{1}{\max(N_d, N_a)} \sum_{i=1}^{N_d} \frac{1}{1 + \eta d_i^2}, \tag{36}$$

where N_d and N_a stand for the numbers of detected and actual edge points, respectively, η is a positive constant, and d_i denotes the error distance or deviation of the i-th detected edge pixel. Additionally, the algorithm for edge detection is employed by the Sobel edge detector. An important assertion is that, in the sequel, the parameter η in (36) is set to 0.1 for three different models. And the optimal parameter $\mathcal{K}$ tailored in $\alpha(x)$ is devoted to balancing the noise removal and detail preservation abilities.

Firstly, we display the performance of the proposed new model in Figs. 1–3, compared with the classical OSV model and TV-Gabor model, for structure-texture image decomposition. More precisely, Fig. 1 corresponds to the standard test images: Lenna and Barbara, both sized by 256×256 pixels. The first rows of Figs. 2 and 3 show the structural part u decomposed by three different models, respectively, while the second rows present their corresponding textural component v. Here, we remark that two original images displayed in Fig. 1 are processed by three models with the equivalent regularization coefficient $\lambda = 2.0$. Complementally, the results exhibited in the first columns of Figs. 2 and 3 are produced by the OSV model with $\gamma = 0.05$. The images obtained via the TV-Gabor model are reported with $\Delta t = 0.001$, while our results are implemented by setting the parameters $\gamma = 0.02, \mathcal{K} = 0.005$, and $\sigma = 0.5$.

As can be seen, Figs. 2 and 3 distinctly illuminate that the images decomposed by our advanced novel

algorithm possess less structure in the textural part v (namely, more edges are kept in the u component) than those of another two TV regularization schemes. Other comparisons with another two methods, in terms of fewer iterations and less CPU time, also demonstrate the outstanding performance of the proposed approach. These data illustrate that our novel strategy is capable of producing highly accurate solutions, and maintaining more sharp edges and structural features in texture image decomposition.

Secondly, we take the Cameraman image (Fig. 4(a), 256×256 pixels) as an example, and show the performance of different models for image denoising. Figure 4(b) (SNR = 15.90 dB) stands for its degraded image contaminated by Gaussian white noise with standard deviation 10. Subsequently, Figs. 4(c), 4(d) and 4(e) denote the recovered cartoon components by employing the OSV model, the TV-Gabor model and our new scheme, respectively. Their corresponding texture and noise components are shown in Figs. 4(f), 4(g) and 4(h). Here we would like to point out that the results presented in Figs. 4(c) and 4(f) are carried out via the conventional TV regularization model, by setting the parameters $\lambda = 0.1$ and $\gamma = 0.05$, while our results displayed in Figs. 4(e) and 4(h) are reported to need 11 iterations with $\lambda = 0.125, \gamma = 0.02, \mathcal{K} = 0.001$, and $\sigma = 0.5$.

Complementally, numerical experiments confirmed that the split Bregman method is much faster than the projection method (Chambolle, 2004), illuminated by Goldstein and Osher (2009, Fig. 5.1). What is more, the same results recovered using our proposed model by the steepest descent algorithm usually consumes 100 iterations ($t = 1.621$ s) and 7 times of CPU time more than the employed numerical algorithm. Table 2, together with these facts, definitely reveals the fast computational speed of the split Bregman technique.

Table 1. Comparison of the recovered results by employing three different models.

Image	Model	SNR	PSNR	FOM
Cameraman	OSV	19.11	31.27	0.9765
	TV-Gabor	19.05	31.25	0.9783
	Our	19.35	31.59	0.9848
Peppers	OSV	16.32	29.93	0.9497
	TV-Gabor	16.21	29.82	0.9531
	Our	16.92	30.56	0.9583

Lastly, in order to further evaluate the reconstruction performance of the proposed strategy, we take the original Peppers image, shown in Fig. 5(a) and sized by 256×256 pixels, as an illustration. Its degenerated version presented in Fig. 5(b) (SNR = 10.97 dB) is corrupted by Gaussian white noise with standard deviation 15. Comparing with the models (1) and (5), we also validate the efficiency of our proposed new methodology. The related simulation results are shown in Fig. 5. More precisely Figs. 5(c), 5(d) and 5(e) individually display the cartoon components of the conventional TV minimization models and our new strategy. The images listed in the third row of Fig. 5 are their corresponding oscillatory components. Thereinto, Figs. 5(c) and 5(f) are run by setting $\lambda = 0.09$ and $\gamma = 0.05$, while Fig. 5(e) is obtained via our proposed algorithm with $\lambda = 0.1, \gamma = 0.02, \mathcal{K} = 0.001$, and $\sigma = 1$ for 12 iterations.

Table 2. Iteration counts and CPU time for three different methods.

Image	Model	N_{iter}	Time (sec.)
Cameraman	OSV	12	0.2186
	TV-Gabor	15	0.4203
	Our	11	0.2089
Peppers	OSV	13	0.2351
	TV-Gabor	15	0.4432
	Our	12	0.2242

As might be expected, it follows from Figs. 4, 5 and Tables 1, 2 that the results recovered by applying the proposed model possess higher SNR, PSNR and FOM values than those of the OSV model and the TV-Gabor model. In other words, our new model performs better in the denoising case.

In conclusion, the provided numerical simulations again indicate the unexampled performance of the proposed scheme, in preserving important structure features and sharp edges in comparison with other variational models.

6. Conclusion

In the current article, based on traditional TV regularization models, we propose an improved spatially and scale adaptive version for edge-preserving image decomposition and restoration. To quickly resolve the advanced variational model, the fast split Bregman method is developed and analyzed minutely. Compared with the existing state-of-the-art OSV model and the TV-Gabor model, related numerical results demonstrate the competitive performance of the proposed strategy in image decomposition and denoising, especially in preserving the fine edge details, and achieving higher image quality.

Acknowledgment

The authors would like to thank the anonymous reviewers for their helpful comments and valuable suggestions. This research was supported by the Hunan Provincial Natural Science Foundation of China (14JJ3105) and

(a) (b)

Fig. 1. Original image: Lenna (a), Barbara (b).

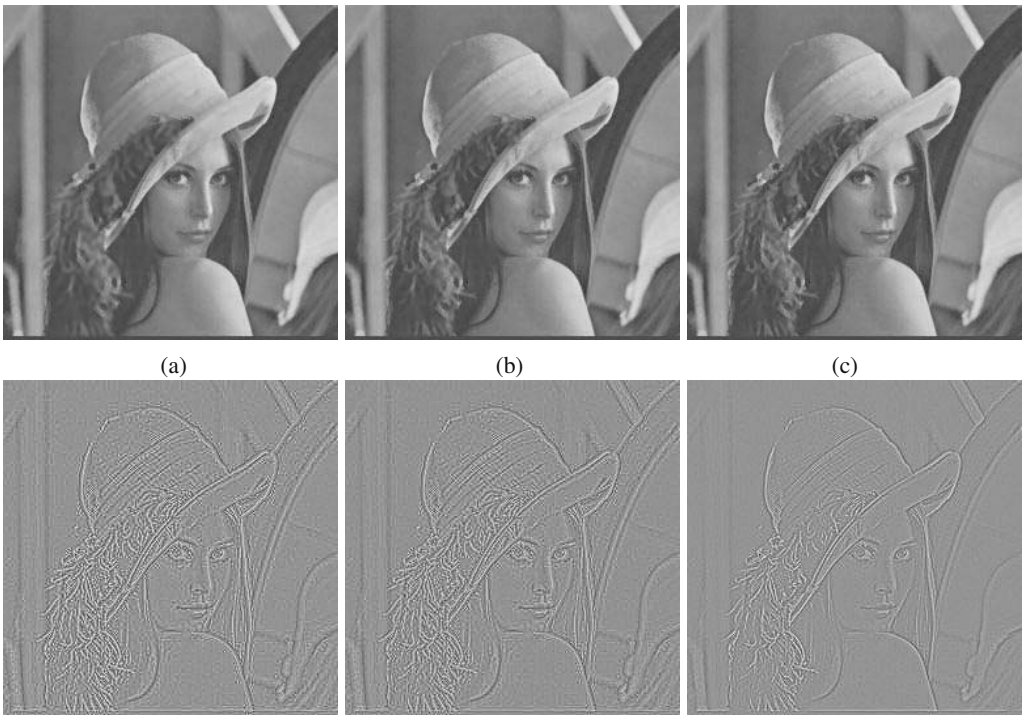

(a) (b) (c)

(d) (e) (f)

Fig. 2. Decomposed cartoon component u and texture component v by using the OSV model ($N_{\text{iter}} = 5$, $t = 0.1795$ s), the TV-Gabor model ($N_{\text{iter}} = 10$, $t = 0.2668$ s) and our proposed $ATV - H^{-1}$ scheme ($N_{\text{iter}} = 3$, $t = 0.1690$ s), respectively: u_{OSV} (a), $u_{\text{TV-Gabor}}$ (b), $u_{\text{ATV-H}^{-1}}$ (c), v_{OSV} (d), $v_{\text{TV-Gabor}}$ (e), $v_{\text{ATV-H}^{-1}}$ (f).

the Scientific Research Fund of the Hunan Provincial Education Department (13C320).

References

Aujol, J.-F., Aubert, G., Blanc-Féraud, L. and Chambolle, A. (2005). Image decomposition into a bounded variation component and an oscillating component, *Journal of Mathematical Imaging and Vision* **22**(1): 71–88.

Aujol, J.-F., Gilboa, G., Chan, T. and Osher, S. (2006). Structure-texture image decomposition—modeling, algorithms, and parameter selection, *International Journal of Computer Vision* **67**(1): 111–136.

Aujol, J.-F. and Gilboa, G. (2006). Constrained and SNR-based solutions for TV-Hilbert space image denoising, *Journal of Mathematical Imaging and Vision* **26**(1–2): 217–237.

Barcelos, C.A.Z. and Chen Y. (2000). Heat flows and related minimization problem in image restoration, *Computers & Mathematics with Applications* **39**(5–6): 81–97.

Cai, J.F., Osher, S. and Shen, Z. (2009). Split Bregman methods and frame based image restoration, *CAM Report 09-28*, UCLA, Los Angeles, CA.

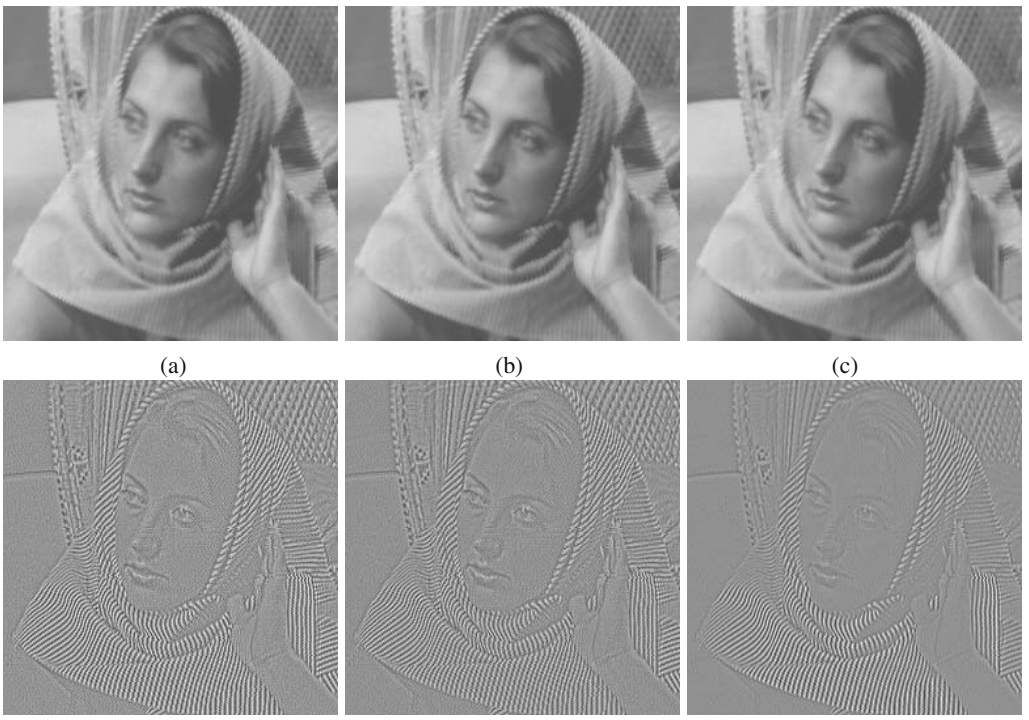

Fig. 3. Decomposed cartoon component u and texture component v by using the OSV model ($N_{\text{iter}} = 4$, $t = 0.1756$s), the TV-Gabor model ($N_{\text{iter}} = 10$, $t = 0.2786$ s) and our proposed $ATV - H^{-1}$ scheme ($N_{\text{iter}} = 4$, $t = 0.1705$ s), respectively: u_{OSV} (a), $u_{\text{TV}-\text{Gabor}}$ (b), $u_{ATV-H^{-1}}$ (c), v_{OSV} (d), $v_{\text{TV}-\text{Gabor}}$ (e), $v_{\text{ATV}-\text{H}^{-1}}$ (f).

Chambolle, A. (2004). An algorithm for total variation minimization and application, *Journal of Mathematical Imaging and Vision* **20**(1–2): 89–97.

Chan, T.F., Golub, G.H. and Mulet, P. (1999). A nonlinear primal-dual method for total variation-based image restoration, *SIAM Journal on Scientific Computing* **20**(6): 1964–1977.

Chan, T.F., Esedoglu, S. and Park, F.E. (2007). Image decomposition combining staircase reducing and texture extraction, *Journal of Visual Communication and Image Representation* **18**(6): 464–486.

Chen, Y. and Wunderli, T. (2002). Adaptive total variation for image restoration in BV space, *Journal of Mathematical Analysis and Applications* **272**(1): 117–137.

Daubechies, I. and Teschke, G. (2005). Variational image restoration by means of wavelets: Simultaneous decomposition, deblurring and denoising, *Applied and Computational Harmonic Analysis* **19**(1): 1–16.

Goldstein, T. and Osher, S. (2009). The split Bregman algorithm for L^1 regularized problems, *SIAM Journal on Imaging Sciences* **2**(2): 323–343.

Hajiaboli, M.R. (2010). A self-governing fourth-order nonlinear diffusion filter for image noise removal, *IPSJ Transactions on Computer Vision and Applications* **2**: 94–103.

Jia, R.-Q., Zhao, H. and Zhao, W. (2009). Convergence analysis of the Bregman method for the variational model of image denoising, *Applied and Computational Harmonic Analysis* **27**(3): 367–379.

Liu, X. and Huang, L. (2010). Split Bregman iteration algorithm for total bounded variation regularization based image deblurring, *Journal of Mathematical Analysis and Applications* **372**(2): 486–495.

Liu, X., Huang, L. and Guo, Z. (2011). Adaptive fourth-order partial differential equation filter for image denoising, *Applied Mathematics Letters* **24**(8): 1282–1288.

Liu, X. and Huang, L. (2012). Total bounded variation based Poissonian images recovery by split Bregman iteration, *Mathematical Methods in the Applied Sciences* **35**(5): 520–529.

Liu, X. and Huang, L. (2013). Poissonian image reconstruction using alternating direction algorithm, *Journal of Electronic Imaging* **22**(3): 033007.

Liu, X. and Huang, L. (2014). A new nonlocal total variation regularization algorithm for image denoising, *Mathematics and Computers in Simulation* **97**: 224–233.

Meyer, Y. (2001). *Oscillating Patterns in Image Processing and Nonlinear Evolution Equations*, University Lecture Series, Vol. 22, AMS, Providence, RI.

Ng, M.K., Yuan, X.M. and Zhang, W.X. (2013). A coupled variational image decomposition and restoration model for blurred cartoon-plus-texture images with missing pixels, *IEEE Transactions on Image Processing* **22**(6): 2233–2246.

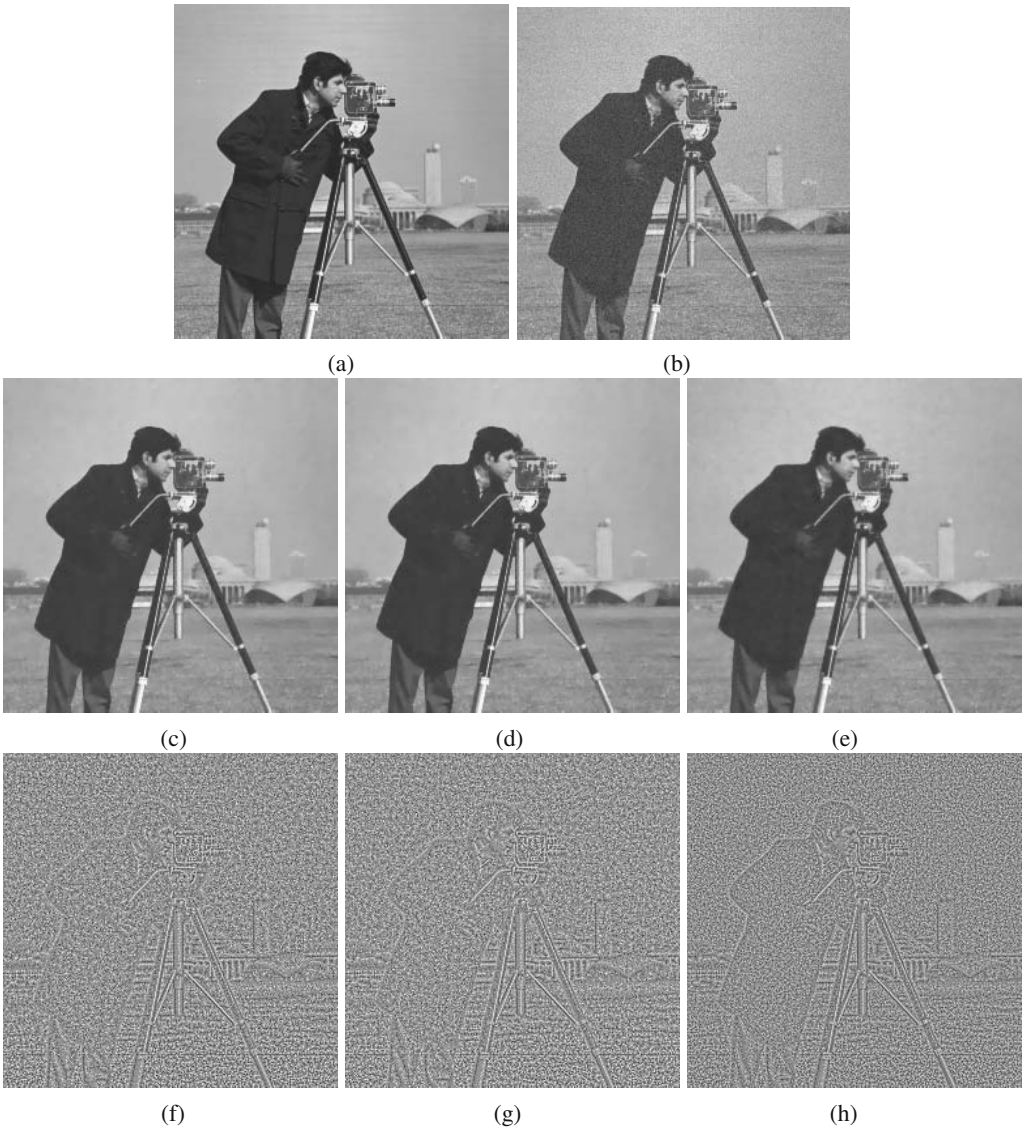

Fig. 4. Recovered structure part u and noise component v by using the OSV model, the TV-Gabor model and our proposed $ATV-H^{-1}$ scheme, respectively: original image (a), noisy image (b), u_{OSV} (c), $u_{\mathrm{TV-Gabor}}$ (d), $u_{\mathrm{ATV-H^{-1}}}$ (e), v_{OSV} (f), $v_{\mathrm{TV-Gabor}}$ (g), $v_{\mathrm{ATV-H^{-1}}}$ (h).

Osher, S., Solé, A. and Vese, L. (2003). Image decomposition and restoration using total variation minimization and H^{-1} norm, *Multiscale Modeling & Simulation* **1**(3): 349–370.

Prasath, V.B.S. (2011). A well-posed multiscale regularization scheme for digital image denoising, *International Journal of Applied Mathematics and Computer Science* **21**(4): 769–777, DOI: 10.2478/v10006-011-0061-7.

Rudin, L., Osher, S. and Fatemi, E. (1992). Nonlinear total variation based noise removal algorithms, *Physica D* **60**(1–4): 259–268.

Setzer, S., Steidl, G. and Teuber T. (2010). Deblurring Poissonian images by split Bregman techniques, *Journal of Visual Communication and Image Representation* **21**(3): 193–199.

Strong, D.M. and Chan, T.F. (1996). Spatially and scale adaptive total variation based regularization and anisotropic diffusion in image processing, *CAM Report 96-46*, UCLA, Los Angeles, CA.

Szlam, A., Guo, Z. and Osher S. (2010). A split Bregman method for non-negative sparsity penalized least squares with applications to hyperspectral demixing, *CAM Report 10-06*, UCLA, Los Angeles, CA.

Vese, L. and Osher, S. (2003). Modeling textures with total variation minimization and oscillating patterns in image processing, *Journal of Scientific Computing* **19**(1–3): 553–572.

Wang, Y., Yang, J., Yin, W. and Zhang, Y. (2007). A new alternating minimization algorithm for total variation

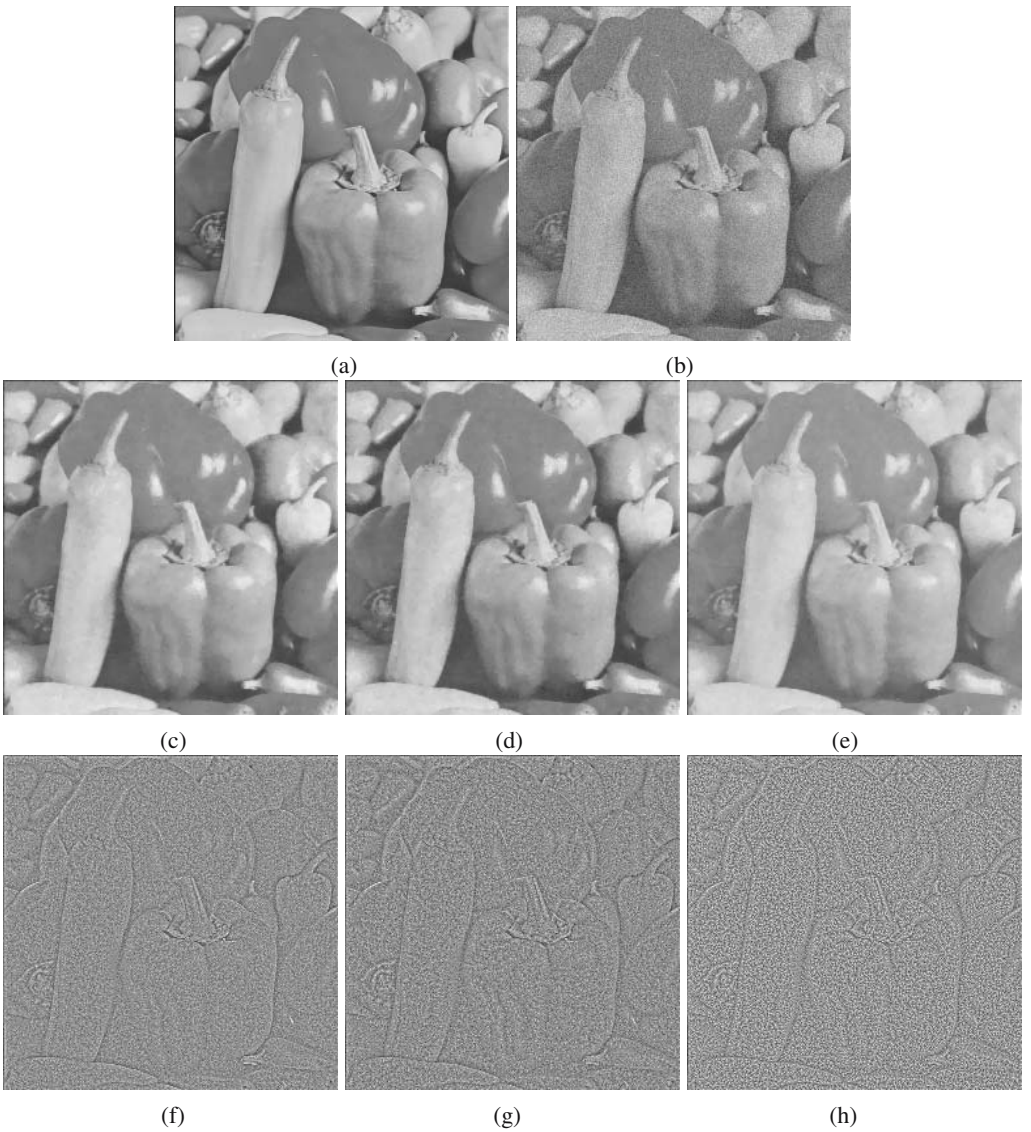

Fig. 5. Recovered structure part u and noise component v by using the OSV model, the TV-Gabor model and our proposed $ATV-H^{-1}$ scheme, respectively: original image (a), noisy image (b), u_{OSV} (c), $u_{\mathrm{TV-Gabor}}$ (d), $u_{\mathrm{ATV-H^{-1}}}$ (e), v_{OSV} (f), $v_{\mathrm{TV-Gabor}}$ (g), $v_{\mathrm{ATV-H^{-1}}}$ (h).

image reconstruction, *CAAM Technical Report, TR07–10*, Rice University, Houston, TX.

Zhang, X., Burger, M., Bresson, X. and Osher, S. (2009). Bregmanized nonlocal regularization for deconvolution and sparse reconstruction, *CAM Report 09-03*, UCLA, Los Angeles, CA.

Xinwu Liu received the Ph.D. degree in applied mathematics from Hunan University, Changsha, China, in 2011. He now works at the School of Mathematics and Computational Science, Hunan University of Science and Technology, Xiangtan, China. The main topics of his current research concern numerical optimization, the theory and applications of differential equations, and image processing and analysis based on partial differential equations.

Lihong Huang received the Ph.D. degree in applied mathematics from Hunan University, Changsha, China, in 1994. He is now a professor at the College of Mathematics and Econometrics, Hunan University, as well as the Department of Information Technology, Hunan Women's University, Changsha. He is the author or a co-author of more than 200 journal papers, and ten edited books. His research interests include dynamics of neural networks, and the theory and applications of differential and difference equations.

Received: 18 April 2013
Revised: 6 January 2014
Re-revised: 28 January 2014